Bone 160 (2022) 116421

Contents lists available at ScienceDirect

Bone

journal homepage: www.elsevier.com/locate/bone

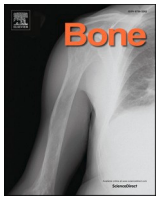

Case Report

Periarticular calcifications containing giant pseudo-crystals of francolite in skeletal fluorosis from 1,1-difluoroethane "huffing"☆,☆☆

Nilton Salles Rosa Neto [a,b,1], Daniel Englert [c], William H. McAlister [d], Steven Mumm [a,b], David Mills [e], Deborah J. Veis [a,b], Alan Burshell [c], Alan Boyde [e,2], Michael P. Whyte [a,b,*,2]

[a] Division of Bone and Mineral Diseases, Department of Internal Medicine, Washington University School of Medicine, St. Louis, MO 63110, USA
[b] Center for Metabolic Bone Disease and Molecular Research, Shriners Hospitals for Children – St. Louis, St. Louis, MO 63110, USA
[c] Endocrinology Department, Ochsner Medical Center, New Orleans, LA 70121, USA
[d] Pediatric Radiology Section, Mallinckrodt Institute of Radiology at St. Louis Children's Hospital, Washington University School of Medicine, St. Louis, MO 63110, USA
[e] Dental Physical Sciences, Dental Institute, Barts and The London School of Medicine and Dentistry, Queen Mary University of London, London, E1 4NS, UK

ARTICLE INFO

Keywords:
Alkaline phosphatase
ALPL gene
Compressed air duster
Difluoroethane
Ectopic calcification
Exostoses
Fluorapatite
Fluoride
Fluorocarbon
Fluorosis
Francolite
Heterotopic calcification
"Huffing"
Hydroxyapatite
Hyperostosis
Hypophosphatasemia
Hypophosphatasia
Metabolic bone disease
Mineralization
Osteosclerosis

ABSTRACT

Inhalant use disorder is a psychiatric condition characterized by repeated deliberate inhalation from among a broad range of household and industrial chemical products with the intention of producing psychoactive effects. In addition to acute intoxication, prolonged inhalation of fluorinated compounds can cause skeletal fluorosis (SF). We report a young woman referred for hypophosphatasemia and carrying a heterozygous *ALPL* gene variant (c.457T>C, p.Trp153Arg) associated with hypophosphatasia, the heritable metabolic bone disease featuring impaired skeletal mineralization, who instead suffered from SF. Manifestations of her SF included recurrent articular pain, axial osteosclerosis, elevated bone mineral density, maxillary exostoses, and multifocal periarticular calcifications. SF was suspected when a long history was discovered of 'huffing' a computer cleaner containing 1,1-difluoroethane. Investigation revealed markedly elevated serum and urine levels of F^-. Histopathology and imaging techniques including backscattered electron mode scanning electron microscopy, X-ray microtomography, energy dispersive and wavelength dispersive X-ray emission microanalysis, and polarized light microscopy revealed that her periarticular calcifications were dystrophic deposition of giant pseudo-crystals of francolite, a carbonate-rich fluorapatite. Identifying unusual circumstances of F^- exposure is key for diagnosing non-endemic SF. Increased awareness of the disorder can be lifesaving.

1. Introduction

Skeletal fluorosis (SF) is usually endemic and most prevalent in the Indian subcontinent, China, and Africa. It typically reflects chronic ingestion of high levels of fluoride (F^-) in well water contaminated with F^- leached from volcanic rock [1–3]. Sometimes endemic SF is

☆ Presented in part at: American Society of Bone and Mineral Research 2021 Annual Meeting, October 1–4, 2021, San Diego, CA, USA [J Bone Miner Res 36 (Suppl. 1): S347, 2021].

☆☆ Supported in part by: The Clark and Mildred Cox Inherited Metabolic Bone Disease Research Fund (#3574) at the Barnes-Jewish Hospital Foundation, and Shriners Hospitals for Children (#71004); St. Louis, MO, USA.

* Corresponding author at: Division of Bone and Mineral Diseases, Washington University School of Medicine, Campus Box 8301, 660 S. Euclid Ave., St. Louis, MO 63110, USA.

E-mail addresses: nsalles@yahoo.com (N. Salles Rosa Neto), daniel.englert@ochsner.org (D. Englert), mcalisterw@wustl.edu (W.H. McAlister), smumm@wustl.edu (S. Mumm), d.mills@qmul.ac.uk (D. Mills), dveis@wustl.edu (D.J. Veis), aburshell@ochsner.org (A. Burshell), a.boyde@qmul.ac.uk (A. Boyde), mwhyte@wustl.edu (M.P. Whyte).

[1] Current address: Center for Rare and Immune Disorders, Hospital Nove de Julho, São Paulo, Brazil.

[2] These authors contributed equally.

https://doi.org/10.1016/j.bone.2022.116421
Received 21 February 2022; Received in revised form 3 April 2022; Accepted 8 April 2022
Available online 13 April 2022

explained by persistent consumption of poor quality 'brick' tea [4,5]. Its severity is conditioned by general health, diet, renal capacity to excrete F^-, and calcium or vitamin D deficiency. Prognosis is worse with advanced age, male gender, low socioeconomic status, poor nutrition, and alcohol/tobacco abuse. Non-endemic SF, in contrast, can reflect excessive consumption of commercial black teas [4–6], ingestion of fluoridated toothpaste or mouthwash [7,8], dust inhalation in aluminum smelting, highly fluorinated drugs (e.g., the antifungal voriconazole), and inhalation abuse of fluorinated gases [9]. Whether endemic or non-endemic, but depending on the age-of-onset, SF complications include compromised dentition, bone pain, joint pain and stiffness, fractures, periostitis, deformities, exostoses, and ectopic calcification [10]. Elevated bone mineral density (BMD) is common in SF, and is due to osteosclerosis of trabecular bone, especially within the axial skeleton [11].

Inhalant use disorder [ICD-10-CM F18; DSM-5 305.9 (mild) or 304.60 (moderate or severe)] features repeated inhalation from among a broad range of household and industrial chemical products [12–14]. Practitioners inhale vapors or aerosols within plastic bags held over their mouth and/or nose, from a soaked cloth, or directly from an open container. The desired effects are intoxication or psychoactive expressions. Owing to their high lipid solubility, inhalants are promptly absorbed throughout pulmonary membranes. Lipophilic hydrocarbons have elevated volatility, easily cross the blood-brain barrier, and explain the central nervous effects [15]. Colloquially, the behavior is known as 'huffing', 'sniffing', 'dusting', or 'bagging' depending on how and what is inhaled [16]. Its prevalence, especially among the young, reflects the ready availability of often inexpensive and legally obtainable products [12,17]. In 2018, approximately two million Americans ≥12 years-of-age reported some inhalant use during the previous year; namely 662,000 adolescents 12 to 17 years-of-age; 495,000 young adults 18 to 25 years-of-age, and 846,000 adults 26 years-of-age or older [18]. F^--containing products abused by inhalation can cause acute kidney injury, hepatotoxicity, neurologic deficits, suicide, cardiac arrhythmia, and sudden death [11,19–21].

Hypophosphatasia (HPP) is the inborn-error-of-metabolism caused by pathogenic variants of the *ALPL* gene that encodes the tissue nonspecific isoenzyme of alkaline phosphatase (TNSALP) [22]. Its biochemical hallmark is hypophosphatasemia; i.e., low serum activity of alkaline phosphatase (ALP). Affected individuals and some 'carriers' of such *ALPL* defects have high circulating levels of the TNSALP natural substrates pyridoxal 5′-phosphate (PLP), a vitameric form of vitamin B_6, and inorganic pyrophosphate (PPi), an endogenous inhibitor of mineralization [22]. HPP in adults also features dental complications and, like SF, osteomalacia with bone pain, muscle weakness, and recurrent slowly healing fractures. There can also be calcium pyrophosphate dihydrate (CPPD) deposition, sometimes as asymptomatic chondrocalcinosis, acute or chronic arthritis, enthesopathy, or ectopic calcifications [22–24]. BMD in HPP may be low, normal, or high due to accumulation of osseous tissue, anterior longitudinal ligament calcification, and fractures [25,26].

Herein, a young woman referred for hypophosphatasemia, skeletal and dental disease, and ectopic mineralization concerning for HPP was found to suffer from SF due to relapse of 'huffing' compressed air duster containing 1,1-difluoroethane (DFE). Giant pseudo-crystals of francolite, a carbonate-rich fluorapatite, were identified within her remarkable dystrophic periarticular calcifications.

2. Patient evaluation and research methods

2.1. Presentation and clinical findings

This 27-year-old white woman was referred to us in 2019. Starting around age 10 years she began to experience bilateral knee pain. At the time, she was active at sports and the problem was ultimately attributed to "growing pains" along with hypermobile joints. The discomfort gradually resolved, and she reported no symptoms until age 22 when she began to experience neck pain. Magnetic resonance imaging (MRI) of her cervical spine revealed "bulging discs", which were managed conservatively with ibuprofen and physical therapy. At age 25 years, her right elbow suddenly became red, swollen, stiff, and intensely painful. Symptoms progressed over several hours, but gradually resolved after a few days with conservative treatment. A similar episode followed in an ankle and the left first metatarsophalangeal (MTP) joint. A steroid was injected for presumed gout, yet her serum uric acid level was normal, and she had no risk factors for gout. One month later, a similar episode occurred in her right first MTP joint, which initially improved with conservative management. At age 26 years, symptoms recurred in her left foot. Radiographs disclosed multiple calcifications. One was surgically removed at the right first MTP joint (Fig. 1). Histopathological examination reportedly showed histiocytes and multinucleated giant cells considered compatible with gout, but crystals were not reported, and synovial fluid analysis was not performed. Subsequently, a rheumatologist noted hypophosphatasemia and referred her to us. Serum ALP activity had been normal twice, and low thrice. Her medical history included mild hearing loss, migraine headaches treated with topiramate, and polycystic ovarian syndrome treated with drospirenone and ethinyl estradiol. She denied alcohol or tobacco use. Against the possibility of HPP, her mother said that her daughter had not lost deciduous teeth prematurely or fractured. Review of systems was negative for fevers, weight change, or diarrhea. Her height was 170 cm (67 in), weight 110 kg (243 lb), body mass index 38 kg/m^2, blood pressure 130/86 mmHg, and heart rate 96 beats per minute. Pain in her right foot caused a limp. Her jaw appeared prominent. Multiple hard white bony nodules projected several millimeters from above her maxillary labial and buccal gum lines (Fig. 2). Joint hypermobility was evident from passive apposition of thumbs to the flexor aspect of the forearms, passive hyperextension of the elbows beyond 10°, and passive hyperextension of the knees beyond 10°. Periarticular hard nodules at her hips and left shoulder were palpable, but not visible. Internal and external rotation and flexion caused pain in her lateral hips.

Routine biochemical studies of mineral metabolism revealed normal serum calcium and parathyroid hormone levels (Supplementary Appendix, Table 1). Hypophosphatasemia (serum ALP 44 U/L; Nl 50–136) together with elevated plasma PLP (68.6 ng/mL; Nl 2.1–21.7) at Quest Diagnostics Inc., USA suggested overt or carrier status for HPP [27]. Phosphoethanolamine, a natural substrate of TNSALP, was not assayed. Biomarkers of skeletal turnover (Quest Diagnostics) included normal serum levels of P1NP (procollagen 1 N-terminal peptide) and CTX (C-telopeptide). Her father twice had low serum ALP, but otherwise normal levels. Her mother had persistent hypophosphatasemia (Supplementary Appendix, Table 2).

However, the patient's radiographic findings were not those of HPP (Fig. 3), but instead featured remarkable flocculent calcifications around her hips, and calcification of the right sacrotuberous ligament apparent at its insertion into the ischial tuberosity (Fig. 3C). Focal periosteal excrescences typical of SF were seen at her femurs, knees, tibias, and fibulas. Her spine and pelvis were diffusely osteosclerotic with marginal osteophytes at the ends of vertebral bodies (Fig. 3A,B). Small excrescences of the spinous processes and small paravertebral and ligament calcifications were present. Multiple soft tissue calcifications were also seen around her shoulders, at the first right metacarpal-carpal joint, the left second metacarpophalangeal joint (Supplementary Appendix, Fig. 1), and at the first MTP joint of both feet.

Dual-energy X-ray absorptiometry (DXA; Lunar Prodigy Primo software version 13.20, GE Healthcare, Chicago, IL, USA) revealed elevated BMD *Z*-scores, especially of her axial skeleton: lumbar spine +10.8, femoral neck (left +1.6, right +3.0), and total hip (left + 4.1, right + 4.6). The small soft tissue calcifications in some regions-of-interest should not have impacted the BMD results in the hip (Supplementary Appendix, Fig 2).

Whole-body technetium-99^m bone scan showed extensive abnormal

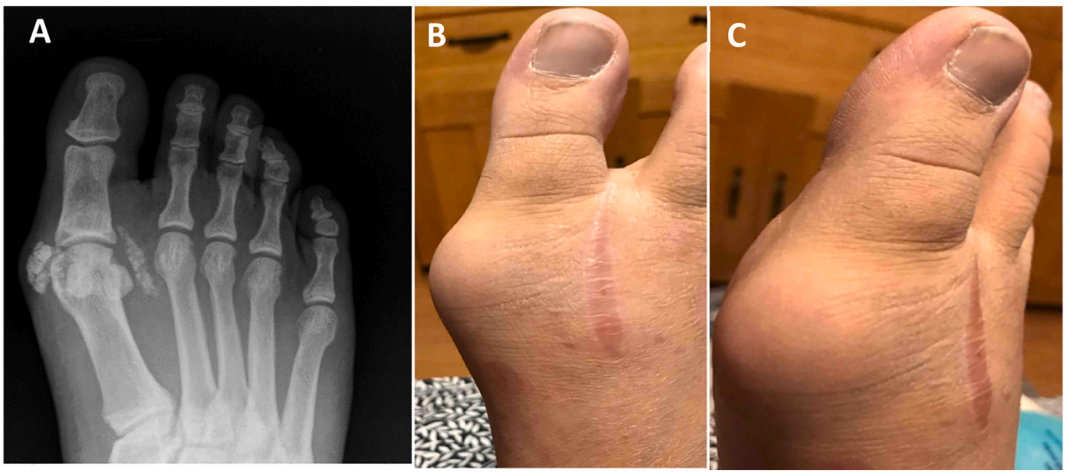

Fig. 1. Right foot radiograph (AP view) and post-surgical photographs.
A) Ectopic calcification around the first right metatarsophalangeal joint.
B, C) The surgical site from which the ectopic calcification was removed for study.

Fig. 2. Maxillary labial and buccal exostoses.
Labial and buccal exostoses are apparent at age 27 years.

radiotracer activity within the heterotopic calcifications adjacent to the glenohumeral joints and hips (Fig. 4). Increased radiotracer activity also involved the medial and lateral femoral condyles and medial and lateral tibial plateau bilaterally, distal tibia, talus, and midfoot bilaterally, and the heterotopic calcification at the right first MTP joint.

MRI of her right hip disclosed soft tissue calcifications surrounding the greater trochanter and throughout the right gluteal musculature, and inflammation within the musculature surrounding the large calcifications. Severe inflammatory changes were present posterior to the greater tuberosity involving the right inferior gemellus, obturator internus, and piriformis muscles. Consistent with diffuse osteosclerosis, decreased bone marrow signal intensities involved the proximal femurs and the pelvic bones. The hip joints were unremarkable, without joint space narrowing, cartilage degeneration, or joint effusion.

Mutation analysis (Blueprint Genetics, Seattle, WA, USA) to test for HPP and tumoral calcinosis assessed *ALPL*, *CLCN5*, *CYP27B1*, *CYP2R1*, *DMP1*, *ENPP1*, *FAH*, *FGF23*, *KL*, *PHEX*, *SCL34A1*, *SCL34A3*, *GALNT3*, and *SAMD9*. Copy-number variation analysis reported no deleterious changes. The positive finding was a single (heterozygous) *ALPL* missense variant in exon 5 (c.457T>C, p.Trp153Arg) previously reported as compound heterozygous in one of our pediatric patients manifesting 'benign prenatal' HPP [22,27,28].

2.2. Family medical history

There was no family history of aortic aneurysms or dissection, or recurrent fractures at young age. Her 68-year-old father, who did not carry her *ALPL* mutation (see below), reported coronary artery bypass grafting and multiple orthopedic problems including spontaneous left biceps tendon rupture, cervical and lumbar spine surgery, and bilateral knee replacement. His plasma PLP level (Quest Diagnostics Inc., USA) was normal, and Invitae Corporation (San Francisco, CA, USA) reported he carried no *ALPL* variant. In contrast, her mother, who had no clinical manifestations typical of HPP, but mild knee osteoarthritis and had undergone medial osteotomy of her left foot for bilateral hallux valgus, was unaware that her medical record documented persistent hypophosphatasemia. We found that she carried her daughter's *ALPL* defect (see below).

2.3. Mutation analyses

Informed written consent for mutation analyses at our research laboratory was obtained from the patient and parents as approved by the Human Research Protection Office, Washington University School of Medicine, St. Louis, MO, USA.

To explore our patient's elevated BMD, leukocyte DNA was studied by Ion Torrent Next Generation Sequencing (NGS) panel (Thermo Fisher Scientific, Waltham, MA, USA) including genes associated with high bone mass and rapid bone turnover: *TNFRSF11A (RANK)*, *TNFRSF11B (OPG)*, *TNFSF11 (RANKL)*, *VCP*, *SQSTM1*, *TGFB1*, *IFITM5*, *MAFB*, *CSF1*, *CSF1R*, *TRAF6*, *RELA*, *RELB*, *REL*, *NFKB1*, *NFKB2*, *TFEB*, *CA2*, *CLCN7*, *CTSK (CATHEPSIN K)*, *OSTM1*, *PLEKHM1*, *TCIRG1*, *SOST*, *SLC29A3*, *LRP4*, *LRP5*, *LRP6*, *SNX10*, *FAM20C*, *FAM123B (AMER1)*, *TYROBP*, *LEMD3*, *DLX3*, and *PTDSS1*. No pathogenic variant was identified.

Sanger-sequencing of all *ALPL* coding exons and adjacent mRNA splice sites along with non-coding exon one confirmed her *ALPL* variant (c.457T>C, p.Trp153Arg), with no other pathogenic variant found [29]. Her pathogenic *ALPL* variant was maternal, not paternal.

2.4. Diagnosis of skeletal fluorosis

During a telephone call from the patient's concerned mother, we learned that her daughter had a history of 'huffing' a compressed air duster, likely containing DFE. From age 18 to 22 years, the patient would inhale as many as 16 cans per day of various brands of product. She then confided resumption of "huffing" six months prior to our initial evaluation. After four months of treatment including inpatient drug

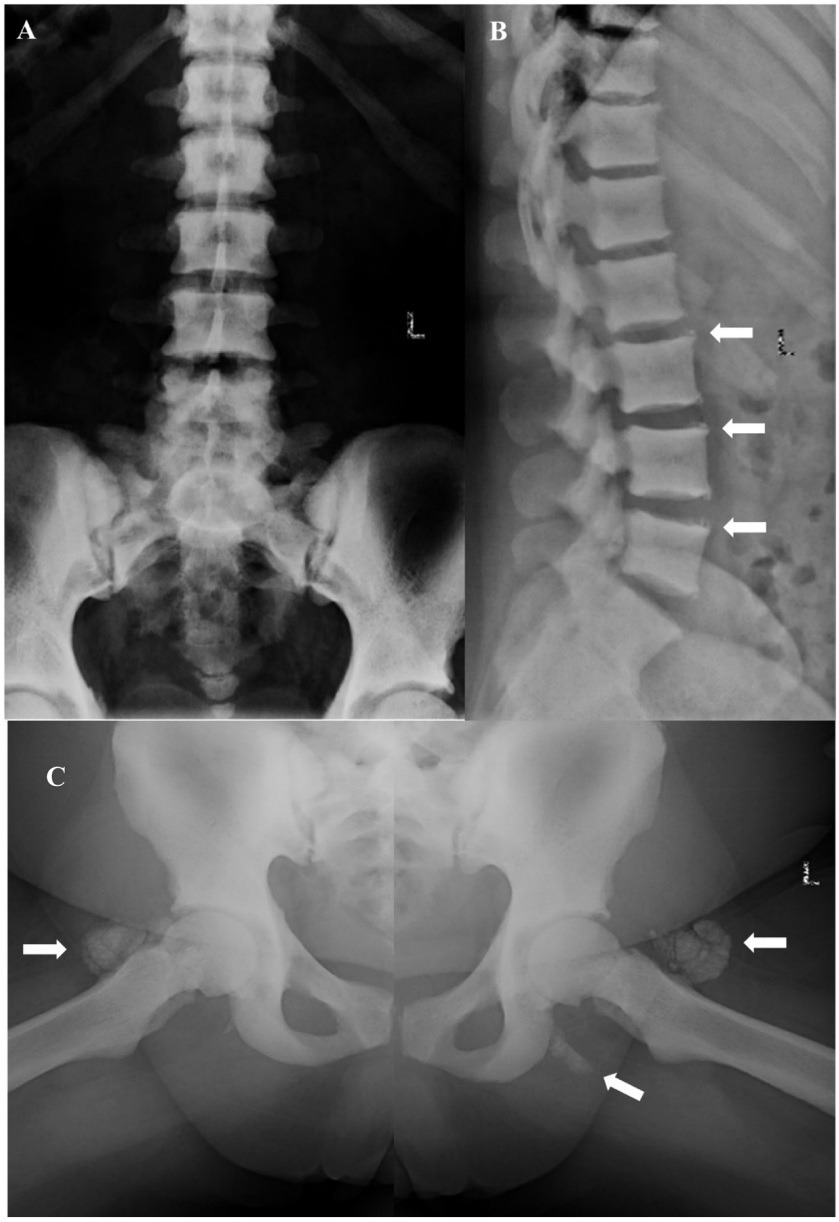

Fig. 3. Anteroposterior (A) and lateral (B) radiographs of the lumbosacral spine, and frog-leg radiograph (C) of the pelvis. The spine and pelvis demonstrate diffuse osteosclerosis. Osteophytes are seen at the cranial and caudal surfaces of the vertebral bodies (white arrows in B) along with small calcifications, excrescences, and ligament calcifications that are not well seen (A and B). The pelvis shows appreciable calcifications around the hip joints (white arrows in C).

rehabilitation, counseling, and psychiatric care, she seemed able to maintain sobriety and reported modest improvement in mobility and pain. However, 'huffing' resumed, complicated by a severe comminuted left distal femur fracture during a fall from standing height and requiring open reduction and internal fixation with an intramedullary rod (Supplementary Appendix, Fig. 3). At the time, serum and spot urine F^- levels were 81.5 μmol/L (reference range < 4.1) and 62 mg/L (reference range 0.2–3.2) [Mayo Clinic Laboratories, USA and Quest Diagnostics, INC, USA; respectively]. Her maxillary exostoses were not a feature of other instances of SF from "huffing" (Fiona J. Cook, MD, Neil Binkley, MD, Joseph Shaker, MD; personal communications).

2.5. Identity of periarticular mineralization

The routine and research methodologies that identified the nature of the ectopic mineralization and tissue removed from the patient's right foot are recounted below and detailed in the Supplementary Appendix. Included were decalcified and non-decalcified histology, scanning electron microscopy (SEM), and X-ray microtomography (XMT) analyses that revealed varying degrees of mineralization within dystrophic calcification. High-contrast resolution XMT showed linear absorption coefficients higher than normal human mineralized tissues. Energy dispersive (EDX) and wavelength dispersive (WDX) X-ray emission microanalyses revealed high levels of fluorine in the denser clusters. X-ray diffraction (XRD) analysis indicated that the mineral phase belonged to the fluoridated carbonate apatite type designated francolite. The cumulative findings are assessed in the Discussion (Section 3.6).

3. Discussion

Our patient was a diagnostic challenge referred with features of HPP (i.e., hypophosphatasemia, high plasma PLP, skeletal disease including elevated BMD, arthropathy, ectopic calcifications, and a pathogenic *ALPL* variant) yet also manifesting maxillary exostoses, periosteal excrescences, osteosclerosis, and remarkable periarticular calcifications. Instead, SF was revealed by eliciting her history of inhalant use disorder involving 1,1-difluoroethane "huffing" and uniquely demonstrating her

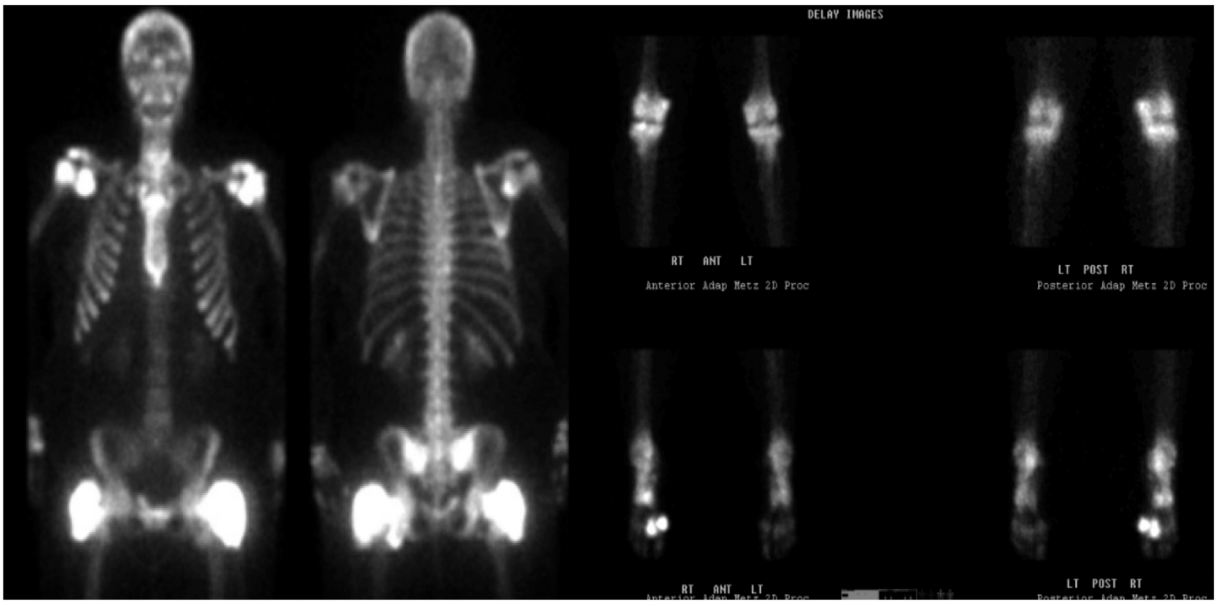

Fig. 4. Whole-body technetium-99^{m} bone scan.
Extensive radiotracer activity is present in the calcifications about the shoulders, sacroiliac joints, hips, knees, ankles, and feet, and around the first MTP joint on the right.

ectopic mineralization contained giant pseudo-crystals of francolite, a carbonate-rich fluorapatite (see below).

3.1. Hypophosphatasia and increased bone mineral density

HPP in adults has diverse radiographic features with broad expressivity [30]. Irrespective of patient age when symptoms began, skeletal imaging may reveal underlying osteomalacic fractures, pseudofractures, delayed fracture consolidation, pseudoarthroses, and osteoarthritis. Seemingly paradoxical ectopic calcification can occur within ligaments, tendons, and cartilage [23,24,30]. BMD may be decreased, normal, or increased [21,26]. Elevated lumbar spine BMD by the areal (gm/cm^2) technique of DXA can reflect excessive bone tissue and ectopic calcification of adjacent structures and ligaments acting as an artifact and usually manifest with aging [25]. In 2021, lumbar spine *Z*-scores up to +8.0 in adults reportedly reflected higher HPP disease burden [25]. Therefore, increased BMD will not distinguish SF from HPP. Mutation analysis of our patient for heritable dense bone disorders, other than HPP, was negative.

3.2. Multifocal periosteal reaction

Periosteal reaction is a nonspecific radiographic finding revealing cortical bone responding to some insult. It may appear rapidly and be aggressive or feature gradual nonaggressive deposition of bone [31]. Among the causes of multifocal periosteal reaction are spondyloarthritis (psoriatic and reactive arthritis); hypertrophic osteoarthropathy (primary or secondary); thyroid acropachy; hypervitaminosis A; scurvy; multiple stress fractures; tumors (benign and malignant bone tumors, metastatic disease, lymphoma, leukemia); chronic recurrent multifocal osteomyelitis; infectious osteomyelitis; syphilis; venous stasis; systemic vasculitis [32]; and prescription drugs, particularly voriconazole, a fluorine-containing antifungal. Periostitis deformans is an extreme example [9], and also not a feature of HPP. Our patient's SF was the apparent cause of her multifocal periosteal reaction.

3.3. Hypophosphatasia and ectopic calcification

Several reports detail the clinical manifestations and radiographic features of the ectopic calcifications that can occur in HPP [23,33–36]. PPi accumulation would explain CPPD disease, leading to acute or chronic arthropathy or asymptomatic chondrocalcinosis [37]. Seemingly paradoxical deposition of hydroxyapatite crystals in periarticular soft tissues can manifest in HPP as “calcific periarthritis” [23]. Our patient had markedly painful periarticular ectopic calcification at multiple sites, and with intense uptake of 99^{m}-Tc during bone scintigraphy. Although she was not hyperphosphatemic, their resemblance to tumoral calcinosis called for mutational analysis for those disorders, which was negative. Extracellular accumulation of PPi, an inhibitor of mineralization, is a biochemical hallmark of HPP and perhaps affected our patient's periarticular calcifications (see below).

Radiographic findings in SF can include axial or generalized osteosclerosis, exostoses, fractures, osteophytes, soft tissue calcification, periostitis, and exuberant periostitis called “periostitis deformans” [38]. Our patient manifested axial osteosclerosis, soft tissue calcification, and periosteal reactions.

3.4. Hypophosphatasia and ALPL variant c.457T>C p.Trp153Arg

Periarticular calcifications occur in adults both with HPP or SF [23,24]. Our patient's persistently hypophosphatasemic mother harbored her daughter's *ALPL* variant (c.457T>C p.Trp153Arg) but any significance concerning her biochemical hallmark for HPP had not been recognized. The only report of her *ALPL* missense change concerns a boy with ‘benign prenatal’ HPP [28] manifesting skeletal disease in utero yet having a mild postnatal course. However, he was compound heterozygous also for *ALPL* c.1183A>G p.Ile395Val. His father carried his son's *ALPL* c.457T>C p.Trp153Arg and had no history of premature tooth loss or fractures, serum ALP 49 U/L (Nl 50–136), normal plasma PLP 73 nM (Nl 5–107), and normal DXA BMD *Z*-scores (lumbar spine −0.2, femoral necks −1.9 and −1.5, and total hips −1.8 and −1.7). Thus, we consider our patient a “carrier” for HPP.

3.5. Inhalant use disorder and skeletal fluorosis

In inhalant abuse disorder, one category of inhaled substances includes haloalkanes or halogenated hydrocarbons; i.e., products containing chlorine (Cl^-) or F^- [13–16]. Typically, the fluorinated products

are considered freon gases [39]. Freon, initially a brand name for dichlorodifluoromethane (Freon R-12), now commonly refers to any fluorocarbon refrigerant gas. Older formulations have been replaced by those less harmful to the ozone layer; e.g., difluoromethane (R-32), and 1,1,2,2-tetrafluoroethane (R-134a), which the automotive industry is gradually replacing with 2,3,3,3-tetrafluoropropene (R-1234yf – not a Freon) for air conditioning because of its low threat for global warming. However, compressed air dusters, also called "computer duster" or "computer cleaner", typically contain 1,1-difluoroethane "(R-152A – DFE). They are readily purchased and are frequently involved in intentional acute intoxication [11]. To deter inhalation, manufacturers can incorporate a bittering agent [40].

Postmortem examination of DFE intoxication has lacked radiographic or histological evaluation of the skeleton [40–45]. Our patient's maxillary exostoses were apparently a unique complication of SF, perhaps reflecting the direct exposure to F^- by 'huffing'. No report provides blood or urine F^- levels. Haloalkanes are not assayed in common drug screen panels, although quantifiable using gas chromatography/mass spectrometry [46,47] in forensic or focused toxicology laboratories.

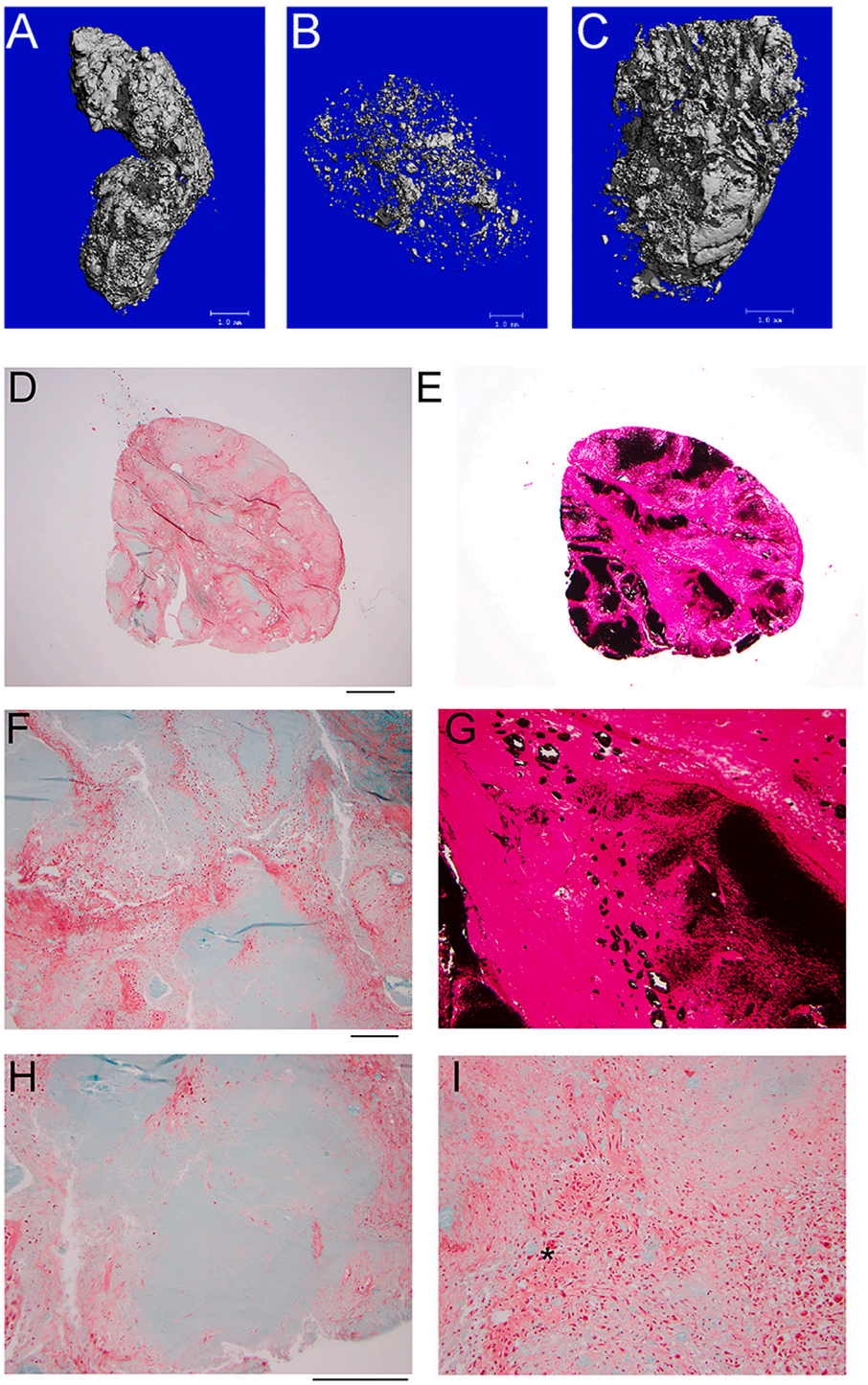

Fig. 5. Scanco X-ray microtomography and histology of fragments of the right foot calcified lesion.
A–C) MicroCT of 3 separate nodules showed variable levels of mineralization, suggesting dystrophic calcification. Scale bars, 1 mm.
Nondecalcified sections of the nodule in C were stained with Goldner's trichrome [mineralized tissue green] (D, F, H, I) or von Kossa [mineralized tissue black] (E, G).
* Indicates a multinucleated cell. Scale bars apply to each row: D–E = 1 mm, F–I = 250 μm. (For interpretation of the references to color in this figure legend, the reader is referred to the web version of this article.)

Studies of healthy volunteers who inhaled DFE to determine its toxicokinetics revealed respiratory absorption and urinary excretion [48]. Rat studies focused on acute changes in different tissue compartments, but not the skeleton [49]. Recently, DFE itself was found and measured in blood 7.8 to 12.8 h (maximum detection time) following suspected acute intoxication [50]. Thus, serum or urinary levels of F^- may reveal fluorinated gas inhalant abuse beyond recent exposure. However, no studies extrapolate acute F^- intoxication to chronic exposure. Sample handling may lead to spurious results because of sample evaporation and F^- losses [50].

3.6. Pseudo-crystals of francolite in skeletal fluorosis

Histological and microCT evaluation of our patient's specimen of heterotopic calcification did not reveal bone tissue, including woven bone or Sharpey fiber bone (Fig. 5). It was not calcified ligament, tendon, or cartilage [51,52]. Her lesions had similarities to: i) the abnormal calcification in soft tissues [53], ii) the formation of high-density mineral infill (HDMI) in micro-cracked bone and articular calcified cartilage, and iii) the formation of high-density mineralized protrusions (HDMP) in hyaline articular cartilage [54–58], all elucidated in the first instance by BSE-SEM. In the dystrophic calcification of juvenile dermatomyositis [53], whilst some of the ectopic mineralization is clearly related to the host soft tissue structure, most of the calcification process seems to exploit inter-fiber space, which we speculate occurs in our patient as the aggregates grow. Closely paralleling what we found in her, we can point to the fusion of innumerable small, unoriented, nearly spherical mineralized domains seen in HDMI and HDMP, where again the existing oriented organic matrix structure is not delineated in the process.

Mineralization in our patient's 'soft tissue' nodules appeared to happen anywhere and everywhere, rather than being centered in the collagen fibers as occurs in bone matrix [59] (Figs. 5–9; Supplementary Appendix, Figs. 4–8). The process begins locally with formation of tiny mineralization centers, which are equidiametrical, i.e., roughly spherical in form and unable to show a morphological orientation. These mineral clusters are extremely numerous with sizes from sub-micron to a few microns in diameter. In poorly mineralized regions, they are separate. In slightly better mineralized regions, they form a continuum, but are still unconnected. In more densely mineralized regions, they fuse to form larger and denser agglomerates and merge to the extent that they form continuous, dense 'pseudo-crystals'. Detail in the BSE-SEM images revealed, however, that these structures form from fused elements.

Growth surfaces of the condensed agglomerates or aggregates had been visualized in 3D after plasma ashing the PMMA-embedded tissue block surface: 3D BSE-SEM images were generated by tilting the sample through 6° between exposures. This showed a wide variety of form according to the way micro-aggregates fused with the enlarging macro-agglomerates – the assembling pseudo-crystals. The plasma-ashed sample was easily disrupted and large and small aggregates collected on an adhesive surface. Most large aggregates had internal voids varying in size from 0.1 to 2 and even 5 μm in diameter. The densest showed few, or no voids, and these seemed most prone to scratching by the polishing abrasives used in sample surface preparation. The voids were more prominent after plasma ashing, which would be explained by suggesting that they had contained an organic matrix residue removed by the process.

Using PLM with thick ground sections from sample A (Supplementary Appendix, Fig. 5, Video 3), we showed these large pseudo-crystals had no preferred orientation. They appeared dark when the through rotation image 'stacks' were processed to make standard deviation images, and they appeared monochrome when these data were used to

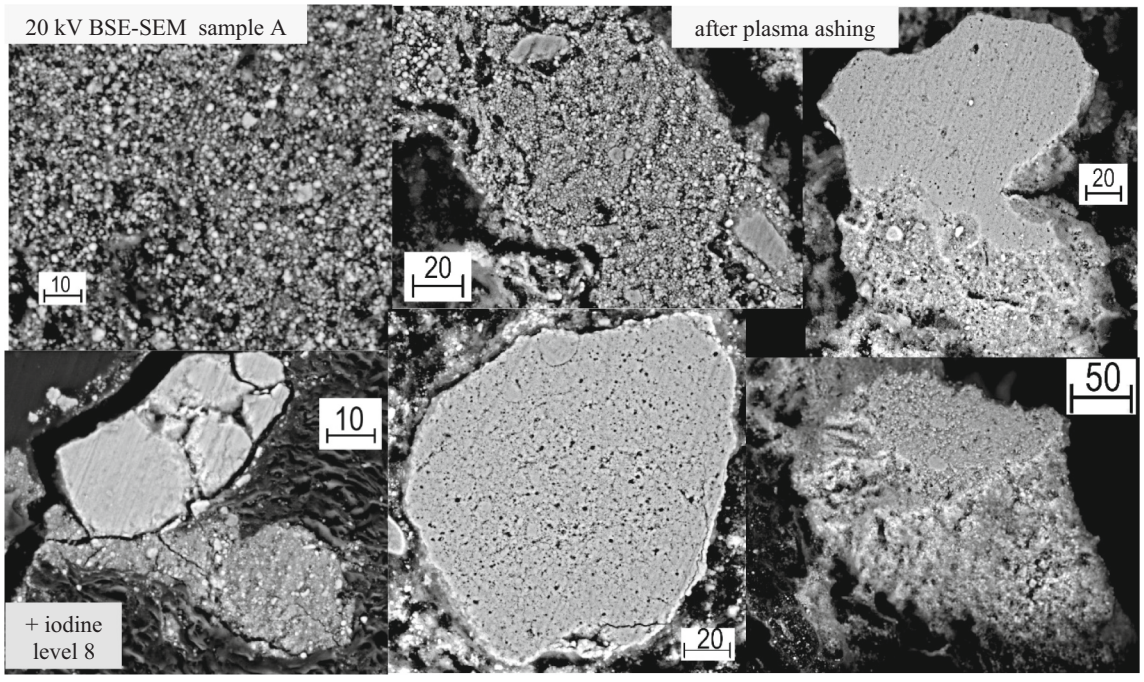

Fig. 6. BSE-SEM sample A.
20 kV BSE-SEM images of sample A, showing detail in surface of PMMA block exposed at different polishing levels. Scale bars in microns.
Top left: Moderately dense packing of small mineral clusters. Level 1.
Bottom left: Dense and less dense clusters. Level 8. Residual iodine staining of soft tissue collagen in background.
Remaining 4 images after plasma ashing at level 8.
Top center: Moderately dense packing of small mineral clusters.
Bottom center: Densely packed region [pseudo-crystal] where join lines between separate components can be recognized, and voids where no mineral is present.
Top right: Dense cluster with both polished surface (top) and growth or fusion surface below.
Bottom right: Less dense aggregate with polished surface top and growth/fusion surface exposed by plasma ashing removal of background matrix below.

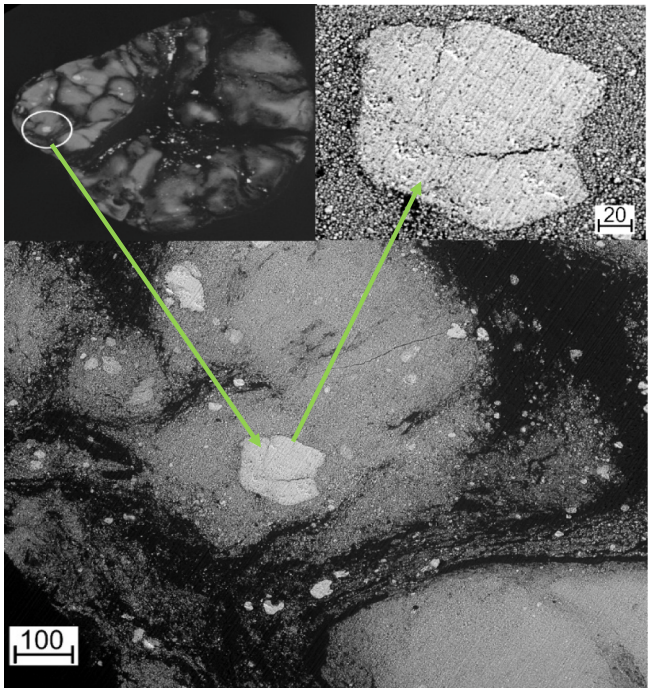

Fig. 7. BSE-SEM and XMT correlation – sample B.
Sample B as microtomed, correlation of high-contrast resolution XMT and BSE-SEM.
[Top left] shows the block surface as seen in high contrast resolution, 7.5 μm voxel size resolution in the QMUL MuCAT XMT scanner. Three slice levels just below the block surface have been averaged. [Bottom center and top right] 20 kV BSE-SEM of the region outlined.
Microtoming the surface caused the linear defects seen in the dense pseudo-crystal cluster: it also rips out small components from the fused mass, leaving a surface in which their morphology is nicely demonstrated.

synthesize the RGB color sequence image. These pseudo-crystals are gigantic on the scale of mineral deposited in bone matrix proper, so large indeed they are easily seen by low magnification light microscopy and SEM and XMT. With the thinner laser microtomy sections of sample B, we could better resolve the smaller elements from which the aggregates are assembled and showed that these are single crystals with polarization extinction minima and brightness maxima and having any spatial orientation (Figs. 5–9; Supplementary Appendix, Figs. 4–8 and Supplementary Video Files). We therefore propose that the lack of orientation in the larger dense aggregates or pseudo-crystals can be attributed to an averaging effect in the bulk. EDX showed the fluorine peak at 0.677 keV by WDX, λ = 1.832 nm. XRD analysis of the microtomed PMMA-embedded block surface suggested that the mineral phase belonged to the fluoridated carbonate apatite type called francolite (Supplementary Appendix, Fig. 7).

High-contrast resolution XMT of periarticular calcifications show linear absorption coefficients in the denser clusters higher than in healthy human mineralized tissues, including, remarkably, dental enamel (Figs. 7–8). Energy-dispersive and wavelength-dispersive X-ray emission document prominent levels of fluorine (Supplementary Appendix, Fig. 6). Application of a novel polarized-light microscope technique assesses samples in this setting. We do not know if this mineralization can resolve with cessation of F^- exposure.

3.7. Treatment

Medical treatment of SF requires that F^- exposure cease [60], but scant information concerns time to recovery [7]. Urine calcium should be monitored because, if there is success, hypercalciuria from negative calcium balance can ensue [7]. Vitamin D and dietary calcium sufficiency are important [11]. Calcium carbonate is commonly given to bind F^- in gastric secretions.

For endemic SF, defluorination by absorption of contaminated water can be achieved with aluminum, ion exchange resins, or lanthanum among other options [61]. Aluminum hydroxide to reduce gastrointestinal (GI) absorption of F^- is not regularly considered in SF [62–65]. Experience from phosphate-binder use for chronic kidney failure suggests sevelamer and lanthanum ion exchange might also bind F^-, however, neither has been studied for SF in animal models or in patients. F^- absorption in inhalant use disorder is expected from the respiratory mucosa and to some unknown extent from the oral mucosa or GI tract. Our patient's soft tissue calcification is a carbonate-rich fluorapatite [66]. Therefore, we wonder if acetazolamide (Diamox®) could be therapeutic by causing a metabolic acidosis.

3.8. Summary

Our report aims to increase awareness and improve recognition and understanding of inhalant use disorder, a common and potentially fatal or debilitating condition. When there is chronic inhalation of F^--containing organic substances, SF can be the result and the medical and social history are key for diagnosis and treatment.

Supplementary data to this article can be found online at https://doi.org/10.1016/j.bone.2022.116421.

CRediT authorship contribution statement

Nilton Salles Rosa Neto: conceptualization, investigation, writing – original draft, review & editing, visualization. **Daniel Englert**: investigation, writing – original draft, review & editing, visualization. **William H. McAlister**: investigation, writing – original draft, review & editing. **Steven Mumm**: methodology, investigation, writing – original draft,

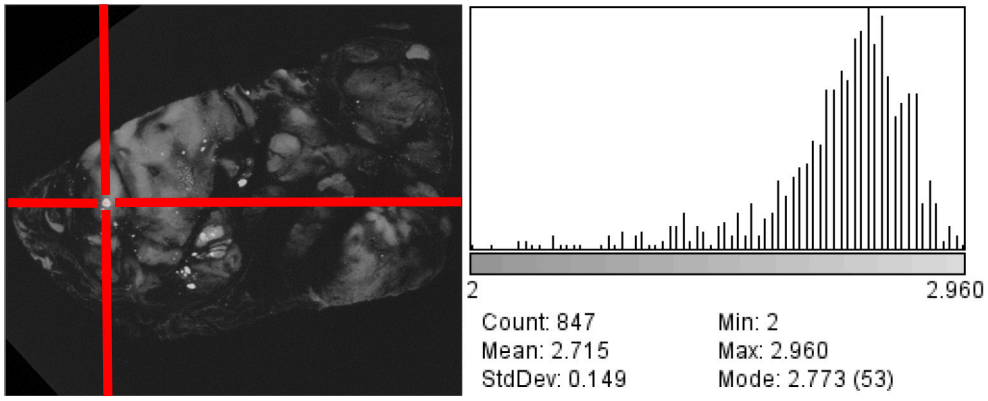

Fig. 8. XMT – ImageJ.
Sample B. High contrast resolution XMT at 7.5 μm nominal spatial resolution. TomView of a single XY plane slice with a dense feature at the intersecting red lines. The region containing this feature was exported as a 3D stack to ImageJ. Linear Absorption Coefficients between 2.00 and 2.96 in 11 × 11 × 7 = 1089 voxels = 459,422 μm^3 centered in marked feature. (For interpretation of the references to color in this figure legend, the reader is referred to the web version of this article.)

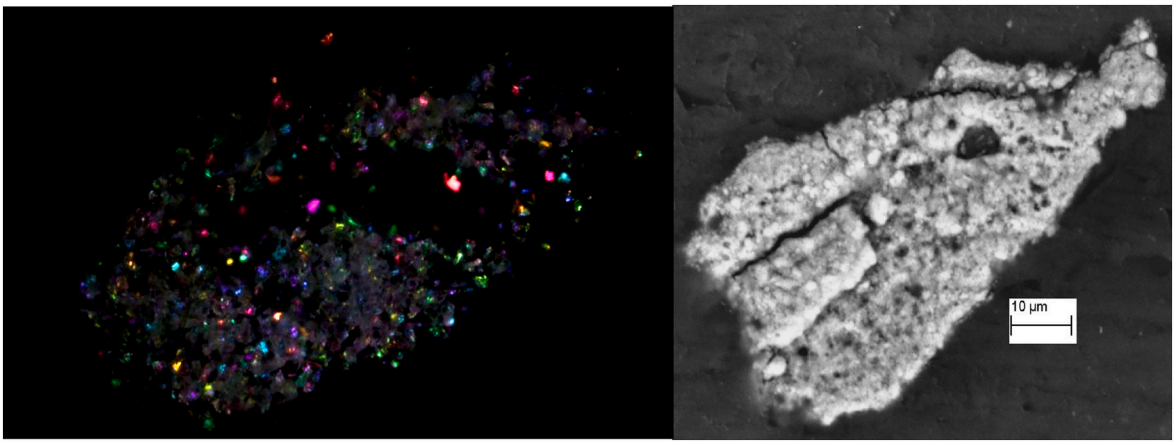

Fig. 9. Correlation of BSE-SEM and new PLM.
Sample B. 30 µm section off block face B made by *LLS Rowiak Laser Microtome*, Hannover, Germany. Correlation of PLM and BSE-SEM. Note that the SEM image is necessarily the surface focus whilst the PLM series is focused inside the section. With the thinner, LAM sections from sample B, we could find regions where there were less densely packed clusters – forming aggregates – where the smallest units could still be resolved. These varied with brightness [i.e., showed extinction and brightness maxima] in the PLM images series taken with rotating crossed polars. In the pseudo-color reconstruction, they have different colors showing that they are single crystals with different orientations. Viewed as video, these crystals show as 'twinkling stars' in the original PLM 'stack' shown in Supplementary Appendix, Video 4. (For interpretation of the references to color in this figure legend, the reader is referred to the web version of this article.)

review & editing. **David Mills**: methodology, investigation, data curation, writing – original draft, review & editing, visualization. **Deborah J. Veis**: methodology, investigation, writing – original draft, review & editing. **Alan Burshell**: investigation, writing – original draft. **Alan Boyde**: conceptualization, methodology, investigation, data curation, writing – original draft, review & editing, visualization, supervision, project administration. **Michael P. Whyte**: conceptualization, investigation, data curation, writing – original draft, review & editing, visualization, supervision, project administration.

Declaration of competing interest

None.

Acknowledgments

We thank Russell Bailey PhD, *FRMS for* examining our samples with EDX and WDX on his high-tech Oxford Instruments equipment, Richard Whiteley M.Eng, D. Phil for the XRD scanning, and Rory M. Wilson, PhD for his help with interpretation of the XRD data. Shenghui Duan performed the *ALPL* gene sequencing and Ion Torrent NGS.

References

[1] G.E. Fabreau, P. Bauman, A.L. Coakley, K. Johnston, K.A. Kennel, J.L. Gifford, H.M. H. Sadrzadeh, G.M. Whitford, M.P. Whyte, G.A. Kline, Skeletal fluorosis in a resettled refugee from Kakuma refugee camp, Lancet 393 (2019) 223–225, https://doi.org/10.1016/S0140-6736(18)32842-3.
[2] World Health Organization, in: J.B.K. Fawell, J. Chilton, E. Dahi, L. Fewtrell, Y. Magara (Eds.), Fluoride in Drinking Water. London, IWA Publishing, UK, 2006 (accessed 09 January 2022), https://www.who.int/water_sanitation_health/publications/fluoride_drinking_water_full.pdf.
[3] S. Srivastava, S.J.S. Flora, Fluoride in drinking water and skeletal fluorosis: a review of the global impact, Curr. Environ. Health Rep. 7 (2020) 140–146, https://doi.org/10.1007/s40572-020-00270-9.
[4] M.P. Whyte, K. Essmeyer, F.H. Gannon, W.R. Reinus, Skeletal fluorosis and instant tea, Am. J. Med. 118 (2005) 78–82, https://doi.org/10.1016/j.amjmed.2004.07.046.
[5] M.P. Whyte, W.G. Totty, V.T. Lim, G.M. Whitford, Skeletal fluorosis from instant tea, J. Bone Miner. Res. 23 (2008) 759–769, https://doi.org/10.1359/jbmr.080101.
[6] K. Izuora, J.G. Twombly, G.M. Whitford, W.G. Totty, R. Pacifici, M.P. Whyte, Skeletal fluorosis from brewed tea, J. Clin. Endocrinol. Metab. 96 (2011) 2318–2324, https://doi.org/10.1210/jc.2010-2891.
[7] E.S. Kurland, R.C. Schulman, J.E. Zerwekh, D.W. Dempster, W.R. Reinus, M. P. Whyte, Recovery from skeletal fluorosis (an enigmatic, american case), J. Bone Miner. Res. 22 (2007) 163–170, https://doi.org/10.1359/jbmr.060912.
[8] E.S. Kurland, M.P. Whyte, Recovery from skeletal fluorosis (reply letter), J. Bone Miner. Res. 22 (2007) 1476, https://doi.org/10.1359/jbmr.070513.
[9] R.J. Tucci, G.M. Whitford, D. Novack, S. Mumm, W.H. McAlister, T.M. Keaveny, M. P. Whyte, Skeletal fluorosis due to inhalation abuse of a difluoroethane-containing computer cleaner, J. Bone Miner. Res. 32 (2017) 188–195, https://doi.org/10.1002/jbmr.2923.
[10] M.M. Patil, B.B. Lakhkar, S.S. Patil, Curse of fluorosis, Indian J. Pediatr. 85 (2018) 375–383, https://doi.org/10.1007/s12098-017-2574-z.
[11] F.J. Cook, M. Seagrove-Guffey, S. Mumm, D.J. Veis, W.H. McAlister, V.N. Bijanki, D. Wenkert, M.P. Whyte, Non-endemic skeletal fluorosis: causes and associated secondary hyperparathyroidism (case report and literature review), Bone 145 (2021), 115839, https://doi.org/10.1016/j.bone.2021.115839.
[12] M.O. Howard, S.E. Bowen, E.L. Garland, B.E. Perron, M.G. Vaughn, Inhalant use and inhalant use disorders in the United States, Addict. Sci. Clin. Pract. 6 (2011) 18–31.
[13] D.G. Barceloux, Fluorinated alkanes, in: D.G. Barceloux (Ed.), Medical Toxicology of Drug Abuse: Synthesized Chemical and Psychoactive Plants, John Wiley & Sons, New Jersey, 2012.
[14] J.V. Bruckner, S. Satheesh Anand, D.A. Warren, Toxic effects of solvents and vapors, in: C.D. Klaassen (Ed.), Casarett & Doull's Toxicology: The Basic Science of Poisons, 9th Ed, McGraw-Hill Education, New York, 2019.
[15] L.M. Tormoehlen, K.J. Tekulve, K.A. Nañagas, Hydrocarbon toxicity: a review, Clin. Toxicol. (Phila.) 52 (2014) 479–489, https://doi.org/10.3109/15563650.2014.923904.
[16] N.J. Connors, Inhalants, https://emedicine. medscape.com/article/ 1174630-overview, in: T.S. Ramachandran (Ed.), Medscape, 2017 (accessed 09 January 2022).
[17] R.N. Lipari, Understanding adolescent inhalant use, https://www.samhsa.gov/data/sites/ default/files/report_3095/ShortReport-3095.html, in: The CBHSQ Report: June 13, 2017, Center for Behavioral Health Statistics and Quality, Substance Abuse and Mental Health Services Administration, Rockville, MD, 2017 (accessed 09 January 2022).
[18] Substance Abuse and Mental Health Services Administration, Key Substance Use and Mental Health Indicators in the United States: Results From the 2018 National Survey on Drug Use and Health (HHS Publication No. PEP19-5068, NSDUH Series H-54), https://www.samhsa.gov/data/sites/ default/files/cbhsqreports/NSDUHNationalFindingsReport2018/NSDUHNationalFindingsReport2018.pdf, Center for Behavioral Health Statistics and Quality, Substance Abuse and Mental Health Services Administration, Rockville, MD, 2019 (accessed 09 January 2022).
[19] J. Avella, J.C. Wilson, M. Lehrer, Fatal cardiac arrhythmia after repeated exposure to 1,1-difluoroethane (DFE), Am J Forensic Med Pathol 27 (2006) 58–60, https://doi.org/10.1097/01.paf.0000202715.71009.0e.
[20] K. Calhoun, L. Wattenbarger, E. Burns, C. Hatcher, A. Khan, A. Patel, M. Badam, Inhaling difluoroethane computer cleaner resulting in acute kidney injury and chronic kidney disease, Case Rep. Nephrol. 2018 (2018), 4627890, https://doi.org/10.1155/2018/4627890.
[21] C.B. Novotny, S. Irvin, E.D. Espiridion, Acute psychosis following 1,1-difluoroethane inhalation, Cureus 11 (2019), e5565, https://doi.org/10.7759/cureus.5565.
[22] M.P. Whyte, Hypophosphatasia - aetiology, nosology, pathogenesis, diagnosis and treatment, Nat. Rev. Endocrinol. 12 (2016) 233–246, https://doi.org/10.1038/nrendo.2016.14.
[23] N. Guañabens, S. Mumm, I. Möller, E. González-Roca, P. Peris, J.L. Demertzis, M. P. Whyte, Calcific periarthritis as the only clinical manifestation of

hypophosphatasia in middle-aged sisters, J. Bone Miner. Res. 29 (2014) 929–934, https://doi.org/10.1002/jbmr.2110.
[24] F.E. McKiernan, R.L. Berg, J. Fuehrer, Clinical and radiographic findings in adults with persistent hypophosphatasemia, J. Bone Miner. Res. 29 (2014) 1651–1660, https://doi.org/10.1002/jbmr.2178.
[25] F. Genest, L. Claußen, D. Rak, L. Seefried, Bone mineral density and fracture risk in adult patients with hypophosphatasia, Osteoporos. Int. 32 (2021) 377–385, https://doi.org/10.1007/s00198-020-05612-9.
[26] R. Desborough, P. Nicklin, F. Gossiel, M. Balasubramanian, J.S. Walsh, A. Petryk, et al., Clinical and biochemical characteristics of adults with hypophosphatasia attending a metabolic bone clinic, Bone 144 (2021), 115795, https://doi.org/10.1016/j.bone.2020.115795.
[27] M.P. Whyte, Hypophosphatasia: enzyme replacement therapy bring new opportunities and new challenges, J. Bone Miner. Res. 32 (2017) 667–675, https://doi.org/10.1002/jbmr.3075.
[28] D. Wenkert, W.H. McAlister, S.P. Coburn, J.A. Zerega, L.M. Ryan, K.L. Ericson, et al., Hypophosphatasia: nonlethal disease despite skeletal presentation in utero (17 new cases and literature review), J. Bone Miner. Res. 26 (2011) 2389–2398, https://doi.org/10.1002/jbmr.454.
[29] S. Mumm, J. Jones, P. Finnegan, P.S. Henthorn, M. Podgornik, M.P. Whyte, Denaturing gradient gel electrophoresis analysis of the tissue non-specific alkaline phosphatase isoenzyme gene in hypophosphatasia, Mol. Genet. Metabol. 75 (2002) 143–153, https://doi.org/10.1006/mgme.2001.3283.
[30] A. Linglart, J.P. Salles, Hypophosphatasia: the contribution of imaging, Arch. Pediatr. 24 (2017), https://doi.org/10.1016/S0929-693X(18)30019-8, 5S74-5S79.
[31] R.S. Rana, J.S. Wu, R.L. Eisenberg, Periosteal reaction, AJR Am. J. Roentgenol. 193 (2009), https://doi.org/10.2214/AJR.09.3300. W259-W272.
[32] F.Y. Yap, M.R. Skalski, D.B. Patel, A.J. Schein, E.A. White, A. Tomasian, et al., Hypertrophic osteoarthropathy: clinical and imaging features, Radiographics 37 (2017) 157–195, https://doi.org/10.1148/rg.2017160052.
[33] A.W. Eade, A.J. Swannell, N. Williamson, Pyrophosphate arthropathy in hypophosphatasia, Ann. Rheum. Dis. 40 (1981) 164–170, https://doi.org/10.1136/ard.40.2.164.
[34] J.D. Macfarlane, H.M. Kroon, A. Cats, Ectopic calcification in hypophosphatasia, Eur. J. Radiol. 6 (1986) 228–230.
[35] A.J. Chuck, M.G. Pattrick, E. Hamilton, R. Wilson, M. Doherty, Crystal deposition in hypophosphatasia: a reappraisal, Ann. Rheum. Dis. 48 (1989) 571–576, https://doi.org/10.1136/ard.48.7.571.
[36] K. Iida, J. Fukushi, T. Fujiwara, Y. Oda, Y. Iwamoto, Adult hypophosphatasia with painful periarticular calcification treated with surgical resection, J. Bone Miner. Metab. 30 (2012) 722–725, https://doi.org/10.1007/s00774-011-0338-9.
[37] K.E. Berkseth, P.J. Tebben, M.T. Drake, T.E. Hefferan, D.E. Jewison, R.A. Wermers, Clinical spectrum of hypophosphatasia diagnosed in adults, Bone 54 (2013) 21–27, https://doi.org/10.1016/j.bone.2013.01.024.
[38] M. Sellami, H. Riahi, K. Maatallah, H. Ferjani, M.C. Bouaziz, M.F. Ladeb, Skeletal fluorosis: don't miss the diagnosis!, Skelet. Radiol. 49 (2020) 345–357, https://doi.org/10.1007/s00256-019-03302-0.
[39] J.W. Elkins, Chlorofluorocarbons (CFCs), in: D.E. Alexander, R.W. Fairbridge (Eds.), The Chapman & Hall Encyclopedia of Environmental Science, Kluwer Academic, Boston, 1999.
[40] Falcon Safety Products, Inc. (n.d.), Inhalant abuse, https://falconsafety.com/product-information/inhalant-abuse/, (accessed 09 January 2022).
[41] L.A. Broussard, T. Brustowicz, T. Pittman, K.D. Atkins, L. Presley, Two traffic fatalities related to the use of difluoroethane, J. Forensic Sci. 42 (1997) 1186–1187.
[42] S.M. Wille, W.E. Lambert, Volatile substance abuse–post-mortem diagnosis, Forensic Sci. Int. 142 (2004) 135–156, https://doi.org/10.1016/j.forsciint.2004.02.015.
[43] T. Hahn, J. Avella, M. Lehrer, A motor vehicle accident fatality involving the inhalation of 1,1-difluoroethane, J. Anal. Toxicol. 30 (2006) 638–642, https://doi.org/10.1093/jat/30.8.638.
[44] C. Vance, C. Swalwell, I.M. McIntyre, Deaths involving 1,1-difluoroethane at the San Diego County medical Examiner's office, J. Anal. Toxicol. 36 (2012) 626–633, https://doi.org/10.1093/jat/bks074.
[45] G. Yamada, M. Takaso, M. Kane, S. Furukawa, M. Hitosugi, A fatality following difluoroethane exposure with blood and tissue concentrations, Clin. Toxicol. (Phila.) 56 (2018) 1167–1168, https://doi.org/10.1080/15563650.2018.1455981.
[46] L.A. Broussard, A. Broussard, T. Pittman, D. Lafferty, L. Presley, Headspace gas chromatographic method for the measurement of difluoroethane in blood, Clin. Lab. Sci. 14 (2001) 3–5.
[47] J. Avella, M. Lehrer, S.W. Zito, A validated method for the quantitation of 1,1-difluoroethane using a gas in equilibrium method of calibration, J. Anal. Toxicol. 32 (2008) 680–687, https://doi.org/10.1093/jat/32.8.680.
[48] L. Ernstgård, B. Sjögren, W. Dekant, T. Schmidt, G. Johanson, Uptake, and disposition of 1,1-difluoroethane (HFC-152a) in humans, Toxicol. Lett. 209 (2012) 21–29, https://doi.org/10.1016/j.toxlet.2011.11.028.
[49] J. Avella, N. Kunaparaju, S. Kumar, M. Lehrer, S.W. Zito, M. Barletta, Uptake and distribution of the abused inhalant 1,1-difluoroethane in the rat, J. Anal. Toxicol. 34 (2010) 381–388, https://doi.org/10.1093/jat/34.7.381.
[50] R. Huet, G. Johanson, 1,1-difluoroethane detection time in blood after inhalation abuse estimated by Monte Carlo PBPK modeling, Pharmaceutics 12 (2020) 997. Erratum in: Pharmaceutics. 13 (2020) 50, https://doi.org/10.3390/pharmaceutics13010050, Correction in: Pharmaceutics. 13 (2021) 1037, https://doi.org/10.3390/pharmaceutics13071037, https://doi.org/10.3390/pharmaceutics12100997.
[51] A. Boyde, Scanning electron microscopic studies of bone, in: G.H. Bourne (Ed.), The Biochemistry and Physiology of Bone, 2nd ed Vol.1, Academic Press, New York, 1972, pp. 259–310.
[52] A. Boyde, S.J. Jones, Scanning electron microscopy of cartilage, in: B.K. Hall (Ed.), Cartilage I, Academic Press, New York, 1983, pp. 105–148.
[53] N. Eidelman, A. Boyde, A.J. Bushby, P.G. Howell, J. Sun, D.E. Newbury, et al., Microstructure and mineral composition of dystrophic calcification associated with the idiopathic inflammatory myopathies, Arthritis Res. Ther. 11 (2009), R159, https://doi.org/10.1186/ar2841.
[54] A. Boyde, C.M. Riggs, A.J. Bushby, B. McDermott, G.L. Pinchbeck, P.D. Clegg, Cartilage damage involving extrusion of mineralisable matrix from the articular calcified cartilage and subchondral bone, Eur. Cell. Mater. 21 (2011) 470–478, https://doi.org/10.22203/ecm.v021a35.
[55] A. Boyde, G.R. Davis, D. Mills, T. Zikmund, T.M. Cox, V.L. Adams, et al., On fragmenting, densely mineralised acellular protrusions into articular cartilage and their possible role in osteoarthritis, J. Anat. 225 (2014) 436–446, https://doi.org/10.1111/joa.12226.
[56] C.J. Ley, S. Ekman, K. Hansson, S. Björnsdóttir, A. Boyde, Osteochondral lesions in distal tarsal joints of icelandic horses reveal strong associations between hyaline and calcified cartilage abnormalities, Eur. Cell. Mater. 25 (2014) 213–236, https://doi.org/10.22203/ecm.v027a16.
[57] C.J. Ley, S. Björnsdóttir, S. Ekman, A. Boyde, K. Hansson, Detection of early osteoarthritis in the centrodistal joints of icelandic horses: evaluation of radiography and low-field magnetic resonance imaging, Equine Vet. J. 48 (2016) 57–64, https://doi.org/10.1111/evj.12370.
[58] A. Boyde, The bone cartilage Interface and osteoarthritis, Calcif. Tissue Int. 109 (2021) 303–328, https://doi.org/10.1007/s00223-021-00866-9.
[59] A. Boyde, S.J. Jones, Aspects of anatomy and development of bone. The nm, μm and mm hierarchy, in: M. Zaidi (Ed.), Molecular and Cell Biology of Bone, Advances in Organ Biology, Vol 5A, JAI Press Inc, Greenwich, Connecticut (publishers), 1998, pp. 3–44.
[60] M.R. Khairnar, A.S. Dodamani, H.C. Jadhav, R.G. Naik, M.A. Deshmukh, Mitigation of fluorosis - a review, J. Clin. Diagn. Res. 9 (2015), https://doi.org/10.7860/JCDR/2015/13261.6085. ZE05-9.
[61] P.Senthil Kumar, S. Suganya, S. Srinivas, S. Priyadharshini, M. Karthika, R. Karishma Sri, Treatment of fluoride contaminated water. A review, Environ. Chem. Lett. 17 (2019) 1707–1726, https://doi.org/10.1007/s10311-019-00906-9.
[62] H. Spencer, L. Kramer, C. Norris, E. Wiatrowski, Effect of aluminum hydroxide on fluoride metabolism, Clin. Pharmacol. Ther. 28 (1980) 529–535, https://doi.org/10.1038/clpt.1980.198.
[63] H. Spencer, L. Kramer, C. Norris, E. Wiatrowski, Effect of aluminum hydroxide on plasma fluoride and fluoride excretion during a high fluoride intake in man, Toxicol. Appl. Pharmacol. 58 (1981) 140–144, https://doi.org/10.1016/0041-008x(81)90124-1.
[64] H. Spencer, L. Kramer, D. Osis, E. Wiatrowski, C. Norris, M. Lender, Effect of calcium, phosphorus, magnesium, and aluminum on fluoride metabolism in man, Ann. N. Y. Acad. Sci. 355 (1980) 181–194, https://doi.org/10.1111/j.1749-6632.1980.tb21337.x.
[65] H. Spencer, D. Osis, M. Lender, Studies of fluoride metabolism in man. A review and report of original data, Sci. Total Environ. 17 (1981) 1–12, https://doi.org/10.1016/0048-9697(81)90103-0.
[66] J. Pinter, G. Lenart, G. Rischak, Physical and chemical investigation of free bodies in articular osteochondromatosis, Acta Orthop. Scand. 50 (1979) 533–535, https://doi.org/10.3109/17453677908989800.